PAN POLSKA AKADEMIA NAUK

METROLOGY AND MEASUREMENT SYSTEMS

Index 330930, ISSN 0860-8229

www.metrology.pg.gda.pl

M&MS

NEW GAS-LIQUID TWO-PHASE FLOW PATTERN MAPS BASED ON THE ENERGY RATIO OF PRESSURE FLUCTUATION THROUGH A VENTURI TUBE

Zhiqiang Sun, Luyang Chen, Fengyan Yao

Central South University, School of Energy Science and Engineering, Changsha 410083, China
(✉ *zqsun@csu.edu.cn*, +86 731 8887 9863, *lychen@csu.edu.cn*, *yaofengyan@csu.edu.cn*)

Abstract

To find effective and practical methods to distinguish gas-liquid two-phase flow patterns, new flow pattern maps are established using the differential pressure through a classical Venturi tube. The differential pressure signal was first decomposed adaptively into a series of *intrinsic mode functions* (IMFs) by the ensemble empirical mode decomposition. Hilbert marginal spectra of the IMFs showed that the flow patterns are related to the amplitude of the pressure fluctuation. The cross-correlation method was employed to sift the characteristic IMF, and then the energy ratio of the characteristic IMF to the raw signal was proposed to construct flow pattern maps with the volumetric void fraction and with the two-phase Reynolds number, respectively. The identification rates of these two maps are verified to be 91.18% and 92.65%. This approach provides a cost-effective solution to the difficult problem of identifying gas-liquid flow patterns in the industrial field.

Keywords: gas-liquid two-phase flow, flow pattern map, Venturi tube, pressure fluctuation, energy ratio, ensemble empirical mode decomposition.

1. Introduction

Gas-liquid two-phase flow is one of the most widely encountered multiphase flow forms in many industrial processes and systems [1–4]. The gas phase and the liquid phase are both easy to deform, and thus it makes the gas-liquid two-phase flow structure very complicated to be recognized [5, 6]. Flow pattern is the description of flow structure in a multiphase flow. Flow pattern is the key factor to properly understand and design a gas-liquid system – it is not only the parameter that influences the heat and mass transfer performance among the gas phase, the liquid phase and the external objects [7], but it is the basis for measurement and evaluation of other parameters in the gas-liquid flow.

So far numerous methods are proposed to perform accurate and effective identification of gas-liquid flow patterns [8, 9]. Among them flow pattern map is a well-accepted approach to prediction of the conditions leading to the transition of flow patterns in a variety of engineering applications. Flow pattern map is generally a two-dimensional diagram with boundaries that distinguish flow patterns from one another. In recent years, some progress has been achieved in the design of gas-liquid flow pattern maps [10–12]. However, determination of boundaries on a flow pattern

Article history: received on Oct. 09, 2018; accepted on Dec. 23, 2018; available online on Jun. 28, 2019; DOI: 10.24425/mms.2019.128352.

map is dependent on the coordinate system adopted. Although a number of coordinate systems are devised, most maps are only valid for a specific set of conditions and/or fluids. Consequently, the development of appropriate coordinate systems is of paramount importance for the design of gas–liquid flow pattern maps.

Among the various types of flow measurement devices ever applied, the Venturi tube has received more popularity because of its small influence on the flow pattern [13]. Venturi tubes consist of a cylindrical "throat" section preceded by a short contraction and followed by a longer expansion to enable pressure recovery. The differential pressure output from a Venturi tube contains rich information about the fluid flow in it. Recently, progress has been achieved in the measurement of gas-liquid two-phase flows using Venturi tubes [14–16], thus making them to be a possible source of signals to construct new coordinate systems of flow pattern maps. To extract imbedded useful information from an acquired signal, an appropriate signal processing method should be selected. The newly proposed *ensemble empirical mode decomposition* (EEMD) is an adaptive technique that decomposes the original signal into a family of *intrinsic mode functions* (IMFs) and a residue, which is based on time scale of the data itself [17, 18]. The EEMD method uses the characteristic of uniform distribution of Gauss white noise to smooth abnormal events such as pulse interference suppression and to suppress mode mixing, so that one can perform the accurate decomposition [19–22].

The purpose of this paper is to identify gas-liquid two-phase flow patterns using the energy ratio of pressure fluctuation through a Venturi tube. The differential pressure signal was first decomposed by EEMD, and then the characteristic IMF was sifted with the cross-correlation method. The energy ratio of the characteristic IMF to the raw signal was applied to construct the flow pattern maps with the volumetric void fraction and the two-phase Reynolds number, respectively. Finally, the identification rates of the new flow pattern maps are verified.

2. Experiments

Experiments were carried out with air and water at ambient temperature and atmospheric pressure. The experimental system, as shown in Fig. 1, was mainly composed of two branches of working fluids and a test section. The air sucked by the compressor and the water pumped from a pool were first pressed into surge tanks to become uniform before their flow rates were measured. The volumetric air flow rate q_{vG} was obtained by the combined use of a vortex flowmeter with 1.0% accuracy and two rotameters both with 1.5% accuracy in view of range abilities. The volumetric

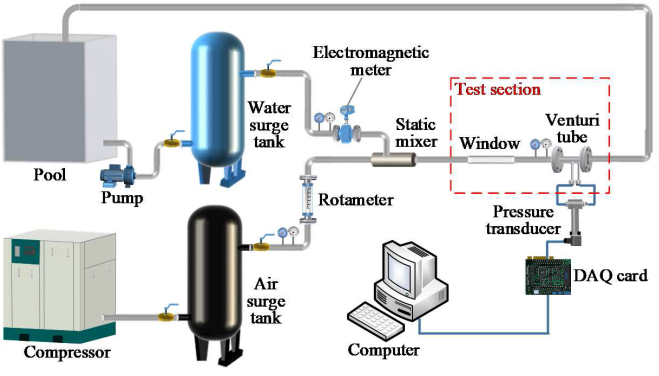

Fig. 1. Experimental system.

water flow rate q_{vL} was acquired by an electromagnetic flowmeter with an accuracy of 0.5%. After their flow rates measured, the air and water were well mixed in a static mixer before they entered the test section horizontally and finally they were recirculated to the pool.

In the test section, a classical Venturi tube was mounted downstream of a transparent window in a circular pipe with an inner diameter $D = 50$ mm. The structure of the Venturi tube used is shown in Fig. 2 with a diameter ratio $\theta = d/D = 0.64$. The differential pressure output from its two pressure tags were measured using a Keller PD-23 type transducer and were sampled by a DAQ card PCL-812PG. The sampling rate of 200 Hz was employed throughout the experiments and 2000 data points were included in each dataset. Through the calibration certified by the Zhejiang Measurement and Test Institute for Quality and Technique Supervision, the discharge coefficient C of the Venturi tube was 0.984 with the accuracy of 0.5% for single-phase water.

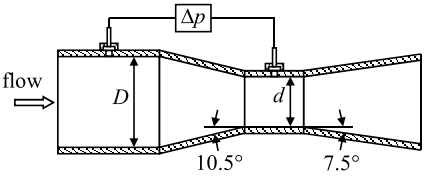

Fig. 2. The Venturi tube used.

A series of experiments were carried out within the ranges of water flow rate 5–18 $m^3 \cdot h^{-1}$ and air flow rate 0–16 $m^3 \cdot h^{-1}$. During each group of the experimental process, the opening of water valve was kept unchanged, while the air flow rates were gradually increased. When a set of experiments were completed, the water valve opening was adjusted to another value and remained fixed again, and the air flow rate was increased. The above processes were repeated until the whole range of water flow rates were covered. Accordingly, by varying the flow rates, three typical gas-liquid two-phase flow patterns were observed through the transparent window, and 173 sets of differential pressure signals were collected in total, which contained 42, 11, 120 sets of bubble, plug and slug flows, respectively.

Some other gas-liquid flow parameters were also obtained, such as the volumetric void fraction β and two-phase Reynolds number Re_{DTP}. The volumetric void fraction reflected the proportion of air and water phases in the flow channel, which were calculated based on two-phase flow rates. The volumetric flow rate of water q_{vL} in the test section was measured directly by the electromagnetic flowmeter in front of the static mixture in view of the negligibility of fluid compressibility. According to the perfect gas equation, the local volumetric flow rates of air in the test section were obtained:

$$q_{vG,\,test} = \frac{q_{vG}(t_{test} + 273.15)(p_G + p_{atm})}{(t_G + 273.15)(p_{test} + p_{atm})} . \tag{1}$$

The total volumetric flow rate $q_{v,\,test}$ was computed by:

$$q_{v,\,test} = q_{vG,\,test} + q_{vL} . \tag{2}$$

Then, β was calculated as follows:

$$\beta = \frac{q_{vG,\,test}}{q_{v,\,test}} . \tag{3}$$

The two-phase Reynolds number was computed by:

$$Re_{DTP} = \frac{Du_{TP}}{\upsilon_{TP}} , \tag{4}$$

$$u_{\mathrm{TP}} = \frac{4q_{\mathrm{v,\,test}}}{\pi D^2}, \tag{5}$$

$$\upsilon_{\mathrm{TP}} = \frac{\mu_{\mathrm{TP}}}{\rho_{\mathrm{TP}}}, \tag{6}$$

$$\mu_{\mathrm{TP}} = \beta\mu_{\mathrm{G}} + (1-\beta)\mu_{\mathrm{L}}, \tag{7}$$

$$\rho_{\mathrm{TP}} = \beta\rho_{\mathrm{G}} + (1-\beta)\rho_{\mathrm{L}}, \tag{8}$$

where u_{TP}, υ_{TP}, μ_{TP} and ρ_{TP} respectively represented the average velocity, kinematic viscosity, dynamic viscosity and density of gas-liquid two-phase flow; μ_{G} and μ_{L} were the dynamic viscosities of gas and liquid phase medium, and ρ_{G} and ρ_{L} were the densities viscosities of gas and liquid phase medium.

3. Results and discussion

3.1. Decomposition of fluctuating differential pressure

Figure 3 shows the raw differential pressure signals of the Venturi tube in the three observed flow patterns as well as the signal in single-phase water flow that was used as a reference. The signals were essentially all fluctuating, but their format and intensity differed from one flow pattern to another. The differential pressure in the bubble flow had relatively small and gentle variation, while in the plug and slug flows, the pressure amplitudes varied considerably violent and intermittent. The time-average values of the differential pressures in the single-phase water, bubble and slug flows were greater than zero; however, negative pressure values appeared in the case of plug flow occasionally. Although there are differences in the time sequences of the signal between each flow pattern, it is hard to discern these flow patterns objectively and quantitatively.

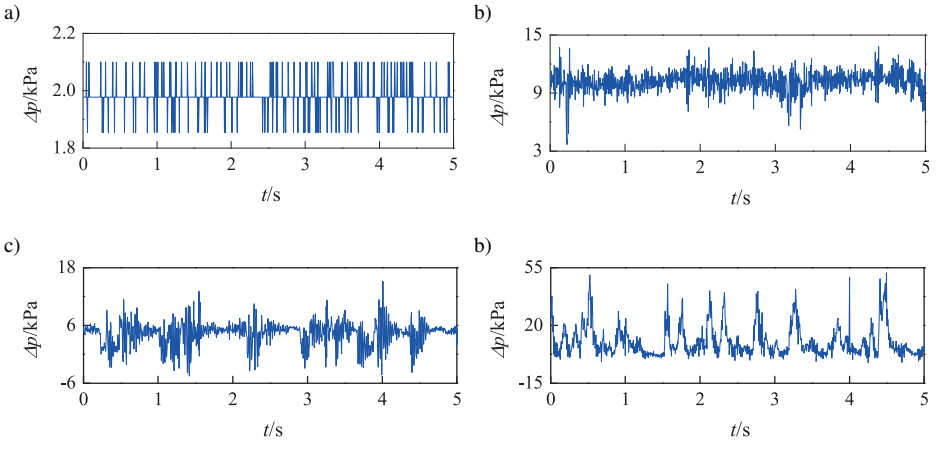

Fig. 3. Raw signals of pressure fluctuation through the Venturi tube in different flow patterns: a) single-phase water flow; b) bubble flow; c) plug flow; d) slug flow.

To reveal underlying components of relevance to the flow patterns in the pressure fluctuation, EEMD was employed to decompose the differential pressure signals. The procedure of EEMD has been presented in our previous papers [23, 24]. Since the length of each sampled pressure signal is 2000 data points, the number of IMFs is lg2000 ≈ 10, which means that nine IMFs and

one residual component can be obtained after EEMD. As shown in Fig. 4, the raw signal Δp, the preceding six IMFs c_1–c_6 and the residual r of each differential pressure are given in different flow patterns. The other three IMFs c_7–c_9 are omitted in later discussion, because the values of

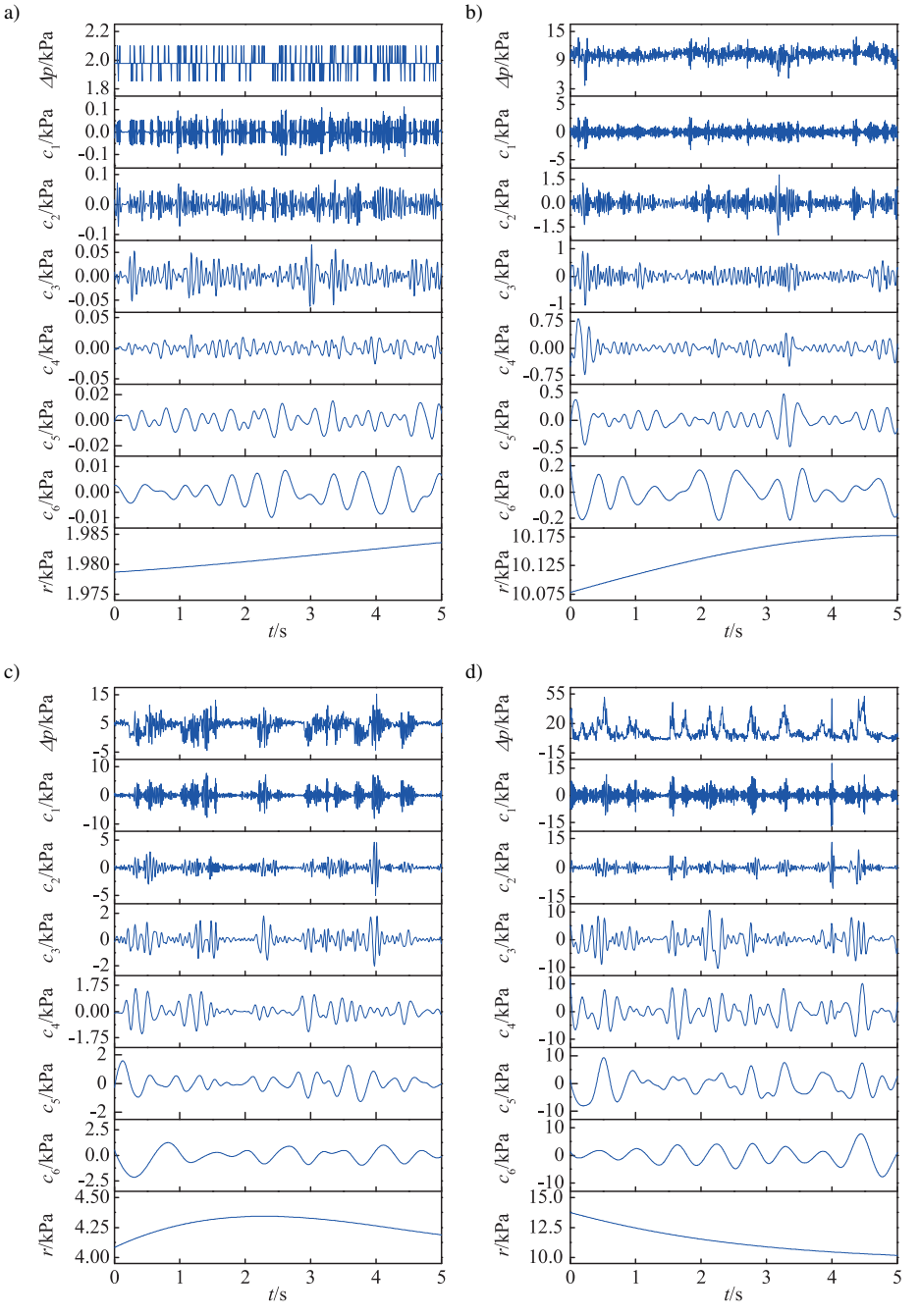

Fig. 4. EEMD results of pressure fluctuation signals in different flow patterns: a) single-phase water flow; b) bubble flow; c) plug flow; d) slug flow.

these components are negligible. It is seen from Fig. 4 that the frequencies of the IMFs in the same signal decrease gradually, and in each series of IMFs there exists a component that resembles the raw signal to some extent and has a relatively larger amplitude than the other IMFs.

3.2. Extraction of characteristic energy ratio

By integrating in time the Hilbert spectrum of each IMF, the Hilbert marginal spectra were obtained, which disclosed the variation of the amplitude of the pressure fluctuation signal in the frequency domain, as shown in Fig. 5. Most amplitudes in the Hilbert marginal spectra were approximate to zero regardless of flow patterns, and the non-zero ones all concentrated in the frequencies less than 10 Hz. Moreover, the non-zero amplitudes appeared in a wider frequency range with the increase of air holdup. There was a distinct difference in the peak amplitude of various flow patterns – the peak value of the single-phase water flow was much smaller than those of the other flows. The strong interaction between the gas and liquid phases caused violent fluctuation in the mixture flows and resulted in a drastic change in the signal amplitude. It reveals that gas-liquid two-phase flow patterns are related to the pressure fluctuation through a Venturi tube.

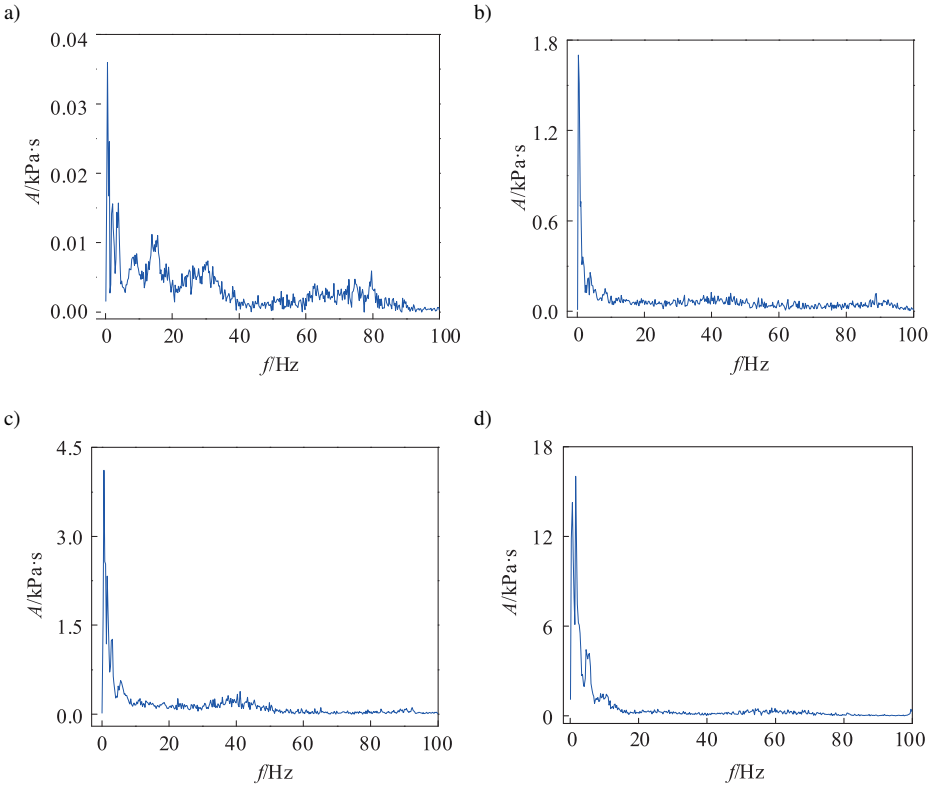

Fig. 5. Hilbert marginal spectra: a) single-phase water flow; b) bubble flow; c) plug flow; d) slug flow.

To find the most relevant component that can be used to discern flow patterns, the cross-correlation method was applied to sift the IMF representing the raw signal to the utmost extent.

The cross-correlation coefficient between the raw signal and each IMF was calculated by [25]:

$$\gamma = \frac{\mathrm{cov}(x, c_j)}{\sqrt{\mathrm{var}(x, x) \cdot \mathrm{var}(c_j, c_j)}}, \tag{9}$$

where var( ) and cov( ) respectively represented the variance and the covariance function, x was the raw signal, and c_j was an IMF. According to this definition, the range of the cross-correlation coefficients was $[-1,\ 1]$.

Due to the orthogonality of IMFs, we defined the IMF of the maximum cross-correlation coefficient as the characteristic IMF, which bore the most similar fluctuation feature to the raw signal. Table 1 lists the cross-correlation coefficients of partial IMFs decomposed from the pressure signals given in Fig. 3. It is clear that the values and distribution of cross-correlation coefficients differed from one flow pattern to another. In the bubble and plug flows, the first IMF c_1 was the characteristic IMF, and their values were markedly greater than those of the other IMFs. As for the slug flow, the difference between each cross-correlation coefficient was indistinctive, and its characteristic IMFc_4 was barely larger than c_5. This is also in agreement with the EEMD results in Fig. 4, which exhibit visually that the characteristic IMF of each flow pattern resembles the raw signal most.

Table 1. Cross-correlation coefficients of partial IMFs in different flow patterns.

Flow pattern	c_1	c_2	c_3	c_4	c_5	c_6
Bubble flow	**0.8237**	0.4209	0.2370	0.1908	0.1732	0.1616
Plug flow	**0.7605**	0.3714	0.2773	0.2989	0.3244	0.3037
Slug flow	0.3807	0.3085	0.4833	**0.5735**	0.5442	0.4707

After the sifting of characteristic IMF, a new quantitative variable, the characteristic energy ratio R, was defined as:

$$R = \frac{E_{\mathrm{IMFC}}}{E_{\mathrm{TOT}}}, \tag{10}$$

$$E_{\mathrm{TOT}} = \sum_{i=1}^{n} E_{\mathrm{IMF}i}, \tag{11}$$

$$E_{\mathrm{IMF}i} = \frac{1}{m} \sum_{k=1}^{m} |c_{ik}(t)|^2, \tag{12}$$

where E_{IMFC} was the energy of the characteristic IMF, E_{TOT} was the total energy of the raw signal, and E_{IMF_i} was the energy of the ith IMF.

3.3. Construction of new flow pattern maps

Flow pattern maps were established based on the characteristic energy ratio. During the construction process, about 80% of the acquired experimental data in each flow pattern were used and were called the construction data. The remaining 20% of the data were used to verify the accuracy of the new flow pattern maps. The numbers of these data are given in detail in Table 2.

Table 2. Numbers of data for constructing the flow pattern maps.

Flow pattern	Total data	Construction data	Verification data
Bubble flow	42	34	8
Plug flow	11	9	2
Slug flow	120	96	24
Total	173	139	34

Figure 6 shows the flow pattern map constructed by using the volumetric void fraction and the characteristic energy ratio as the horizontal and the vertical coordinates. The construction data were first plotted in the coordinate plane, and boundaries were delineated between each flow pattern. The general criterion to delineation was that the central separation lines were employed as far as possible to discern each flow pattern region including both the overlapping and the transitional zones. Then, the construction data were removed and the flow pattern map was shaped finally. Fig. 6a shows that the characteristic energy ratio of the plug flow was distinctly less than those of the bubble and slug flows. To examine the validity, the verification data were plotted on the volumetric void fraction based flow pattern map. If a point of the verification data was located wholly in the region of another flow pattern, it was deemed as a wrong identification. If a verification data point happened to fall on a boundary, it was considered as half-wrong identification. According to this assumption, the identification rate of this flow pattern map was 91.18% (three wrong identifications).

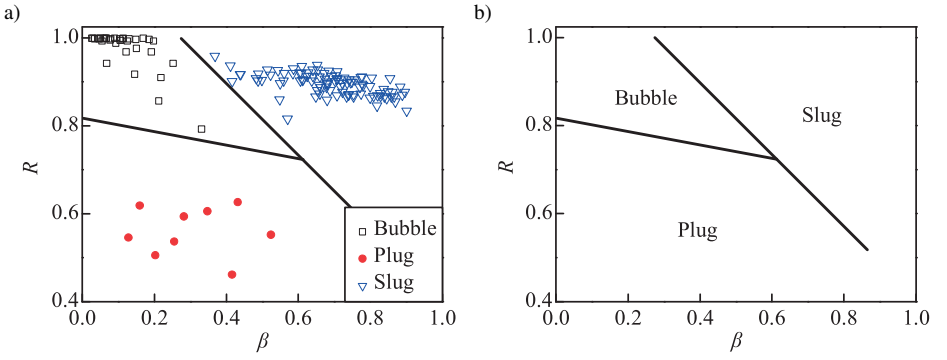

Fig. 6. Volumetric void fraction based flow pattern map: a) with delineated boundaries between each flow pattern; b) with removed construction data to shape the map.

According to the same steps and criterion, the two-phase Reynolds number-based flow pattern map was constructed, as shown in Fig. 7. There were clear boundaries between each of the flow patterns. The identification rate of the developed flow pattern map was 92.65% (two and a half wrong identifications).

The recognition of gas-liquid two-phase flow patterns using the $R - \beta$ and $R - Re_{\mathrm{DTP}}$ maps is affected by many factors and can be further improved. The gas-liquid flow is a time-varying and dynamic process that is severely influenced by phase interactions, pipeline conditions and environmental aspects. The fluctuating differential pressures generated through the Venturi tube are therefore rather complex and can be considered as strong stochastic signals [26]. Since a sample of the fluctuating pressure signal with a finite length is only a snapshot of its ensemble, the features

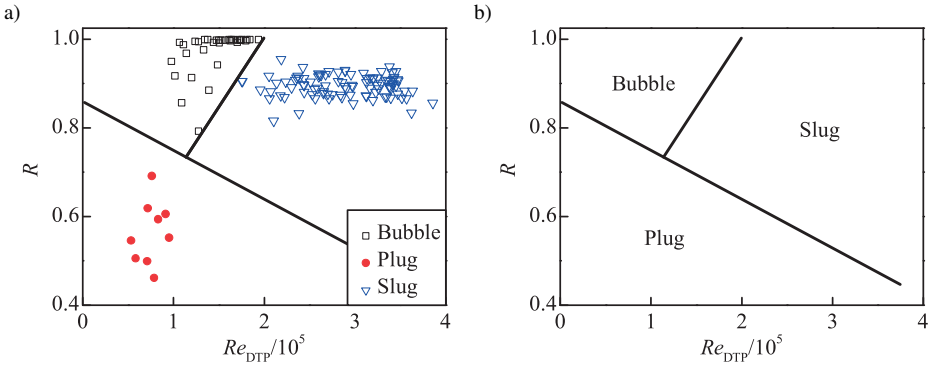

Fig. 7. Two-phase Reynolds number-based flow pattern map: a) with delineated boundaries between each flow pattern; b) with removed construction data to shape the map.

extracted from the sample vary randomly. The gas-liquid flow pattern distinguished from these features is hence fluctuating and time varying [27]. The uncertainty in the determination of flow patterns can be minimized by increasing the sample length of the pressure fluctuation signals; however, the dynamic response of the measurement system would be compromised.

4. Conclusions

In this paper, the differential pressure through a classical Venturi tube was utilized to identify gas-liquid two-phase flow patterns. The main findings are as follows:

1. The differential pressure signal was decomposed adaptively into a number of IMFs by the EEMD method. The Hilbert marginal spectra of these IMFs revealed that the gas-liquid flow patterns are related to the amplitude of the pressure fluctuations.
2. The cross-correlation method was employed to sift the characteristic IMF, that is the maximum cross-correlation coefficient that most resembles the raw differential pressure signal.
3. The energy ratio of the characteristic IMF to the raw signal was proposed to construct the flow pattern maps respectively with the volumetric void fraction and the two-phase Reynolds number. The identification rates of the new $R - \beta$ and $R - Re_{DTP}$ maps were verified to be 91.18% and 92.65%.

This approach is promising because of the absence of expensive devices and complicated configuration for the same application, and provides a cost-effective solution to the difficult problem of identifying gas–liquid flow patterns.

Acknowledgements

We are grateful for the financial support from the National Natural Science Foundation of China (51576213), the Hunan Provincial Natural Science Foundation of China (2017JJ1031), the Changsha Scientific Program (KQ1706066), the Fundamental Research Funds for the Central Universities of Central South University (2018zzts024) and the Open-End Fund for the Valuable and Precision Instruments of Central South University (CSUZC201822).

Nomenclature

A – amplitude
C – discharge coefficient of Venturi tube
c – intrinsic mode function
D – inner diameter of pipe
d – inner diameter of Venturi throat
E – energy of signal
f – frequency
p – pressure
q_m – mass flow rate
q_v – volumetric flow rate
R – characteristic energy ratio
Re_D – Reynolds number
r – residual
t – temperature
u – velocity

Greek Symbols

β – volumetric void fraction
γ – cross-correlation coefficient
θ – diameter ratio
μ – dynamic viscosity
ν – kinematic viscosity
ρ – density

Subscripts and superscripts

atm – standard atmospheric pressure
G – gas phase (air)
IMFC – characteristic IMF
L – liquid phase (water)
test – test section
TOT – total
TP – gas-liquid two-phase flow

Abbreviations

EEMD – ensemble empirical mode decomposition
IMF – intrinsic mode function

References

[1] Roshani, G.H., Nazemi, E., Shama, F., Imani, M.A., Mohammadi, S. (2018). Designing a simple radiometric system to predict void fraction percentage independent of flow pattern using radial basis function. *Metrol. Meas. Syst.*, 25(2), 347–358.

[2] Witkowski, D., Kubicki, W., Dziuban, J.A., Jašíková, D., Karczemska, A. (2018). Micro-particle image velocimetry for imaging flows in passive microfluidic mixers. *Metrol. Meas. Syst.*, 25(3), 441–450.

[3] Huang, S., Yin, J., Sun, Z., Li, S., Zhou, T. (2017). Characterization of gas–liquid two-phase flow by correlation dimension of vortex-induced pressure fluctuation. *IEEE Access*, 5, 10307–10314.

[4] Kumar, A., Bhowmik, S., Ray, S., Das, G. (2017). Flow pattern transition in gas–liquid downflow through narrow vertical tubes. *AICHE J.*, 63(2), 792–800.

[5] Sun, Z., Shao, S., Gong, H. (2013). Gas–liquid flow pattern recognition based on wavelet packet energy entropy of vortex-induced pressure fluctuation. *Meas. Sci. Rev.*, 13(2), 83–88.

[6] Sun, Z., Zhang, H. (2008). Neural networks approach for prediction of gas–liquid two-phase flow pattern based on frequency domain analysis of vortex flowmeter signals. *Meas. Sci. Technol.*, 19(1), 015401.

[7] Li, S., Sun, Z. (2018). Melting of phase change material from an isothermal vertical wall in a semi-enclosure. *Int. J. Heat Mass Transf.*, 127, 1041–1052.

[8] Zhu, H., Li, Z., Yang, X., Zhu, G., Tu, J., Jiang, S. (2017). Flow regime identification for upward two-phase flow in helically coiled tubes. *Chem. Eng. J.*, 308, 606–618.

[9] Jagannathan, N., Chidambaram, B., Seshadri, A., Muniyandi, V. (2015). Characterization of gas–liquid two-phase flows using laser patterns. *Can. J. Chem. Eng.*, 93(9), 1678–1685.

[10] Yang, Z., Chen, G., Zhuang, X., Song, Q., Deng, Z., Shen, J., Gong, M. (2018). A new flow pattern map for flow boiling of R1234ze(E) in a horizontal tube. *Int. J. Multiph. Flow*, 98, 24–35.

[11] Wua, B., Firouzi, M., Mitchell, T., Rufford, TE., Leonardi, C., Towler, B. (2017). A critical review of flow maps for gas-liquid flows in vertical pipes and annuli. *Chem. Eng. J.*, 326, 350–377.

[12] Zhou, Y., Hou, Y., Li, H., Sun, B., Yang, D. (2015). Flow pattern map and multi-scale entropy analysis in 3 ×3 rod bundle channel. *Ann. Nucl. Energy*, 80, 144–150.

[13] Elperin, T., Fominykh, A., Klochko, M. (2002). Performance of a Venturi meter in gas–liquid flow in the presence of dissolved gases. *Flow Meas. Instrum.*, 13(1–2), 13–16.

[14] Wrasse, A.D.N., Bertoldi, D., Morales, R.E.M., Da Silva, M.J. (2017). Two-phase flow rate measurement using a capacitive sensor and a Venturi meter. *The 16th IEEE Sensors Conference*, Glasgow, 822–824.

[15] Xu, Y., Yuan, C., Long, Z., Zhang, Q., Li, Z., Zhang, T. (2013). Research the wet gas flow measurement based on dual-throttle device. *Flow Meas. Instrum.*, 34, 68–75.

[16] Fang, L., Zhang, T. (2008). Performance of a horizontally mounted Venturi in low-pressure wet gas flow. *Chin. J. Chem. Eng.*, 16(2), 320–324.

[17] Li, H., Li, L., Zhao, D. (2018). An improved EMD method with modified envelope algorithm based on C-2 piecewise rational cubic spline interpolation for EMI signal decomposition. *Appl. Math. Comput.*, 335, 112–123.

[18] Zhang, X., Liang, Y., Zhou, J., Zang, Y. (2015). A novel bearing fault diagnosis model integrated permutation entropy, ensemble empirical mode decomposition and optimized SVM. *Measurement*, 69, 164–179.

[19] Chen, B., Yin, P., Gao, Y., Peng, F. (2018). Use of the correlated EEMD and time-spectral kurtosis for bearing defect detection under large speed variation. *Mech. Mach. Theory*, 129, 162–174.

[20] Wang, W., Chau, K., Xu, D., Chen, X. (2015). Improving forecasting accuracy of annual runoff time series using ARIMA based on EEMD decomposition. *Water Resour. Manag.*, 29(8), 2655–2675.

[21] Wang, Y., Yeh, C., Young, H.W.V., Hu, K., Lo, M.T. (2014). On the computational complexity of the empirical mode decomposition algorithm. *Physica A*, 400, 159–167.

[22] Wang, Y., Markert, R., Xiang, J., Zheng, W. (2015). Research on variational mode decomposition and its application in detecting rub-impact fault of the rotor system. *Mech. Syst. Signal Proc.*, 60, 243–251.

[23] Huang, S., Sun, Z., Zhou, T., Zhou, J. (2018). Application of time–frequency entropy from wake oscillation to gas-liquid flow pattern identification. *J. Cent. South Univ.*, 25(7), 1690–1700.

[24] Sun, Z., Gong, H. (2012). Energy of intrinsic mode function for gas-liquid flow pattern identification. *Metrol. Meas. Syst.*, 19(4), 759–766.

[25] Adam, K., Robert, H., Anna, S. (2011). Investigation of the statistical method of time delay estimation based on conditional averaging of delayed signal. *Metrol. Meas. Syst.*, 18(2), 335–342.

[26] Sun, Z. (2010). Mass flow measurement of gas-liquid bubble flow with the combined use of a Venturi tube and a vortex flowmeter. *Meas. Sci. Technol.*, 21(5), 055403.

[27] Sun, Z., Chen, Y., Gong, H. (2012). Classification of gas-liquid flow patterns by the norm entropy of wavelet decomposed pressure fluctuations across a bluff body. *Meas. Sci. Technol.*, 23(12), 125301.